Exploration COMSOL in Modeling RLSA™ CVD Processes in $Ar+H_2+SiH_4+C_2H_6$ and Dopant Gas

Jozef Brcka[1]*, Sundar Gandhi[2], Raymond Joe[2]
[1]Tokyo Electron U.S. Holdings, Inc., U.S. Technology Development Center. 2400 Grove Blvd., Austin, TX 78741, [2]Tokyo Electron America, Inc., 2400 Grove Blvd., Austin, TX 78741
*Corresponding author: jozef.brcka@us.tel.com

Abstract: The plasma reactor with radial line slot antenna (RLSA™), a planar microwave (2.45 GHz) plasma source, is used in etch and deposition technology, typically in reactive rich gaseous environment, and for processes that are sensitive to plasma damage. Besides a strict uniformity control, the plasma chemistry is becoming one of the key challenges in current technology. These two aspects are spatially related due to microwave interaction with electrons in plasma. In this paper, we present a two-dimensional axisymmetric model of microwave plasma produced by RLSA™ source and its numerical implementation under COMSOL Multiphysics software. Mixtures of Ar with H_2, SiH_4 are used for deposition of amorphous or polycrystalline silicone. Content of carbon in film is driven by choice and ratio of hydrocarbons in mixture (adding C2H6 into model). Current model considers 28 species (61 reactions) in plasma and 3 species (17 reactions) on surface of the silicon wafer. The motivation in this work is to explore capabilities of software application and add value to the understanding of physics and chemistry of deposition processes.

Keywords: microwave plasma, CVD, reactor model, silane, multiphysics.

1. Introduction

Typically, microwave plasma conditions are very well suitable for precursor decomposition and generation of radicals and enable low damage processing of the fine features on the silicon wafer. Commercial reactor with radial line slot antenna (RLSA™), a planar microwave (2.45 GHz) plasma source is widely used in etch and deposition[1] (Fig. 1) technology for semiconductor device fabrication. The microwave power is coupled through RLSA™ and dielectric window to plasma. The RLSA™ belongs to a class of surface wave (SW) sustained plasma sources. In semiconductor fabrication the silicon wafers are exposed to a reactive rich plasma environment. Plasma chemistry is one of the key challenges. Besides the source and reactor geometry, the pressure range accessible for SW-excited plasmas will depend also on the process gas composition. Scaled up chamber diameters allow operating pressure range to be reduced in case of SW mode.

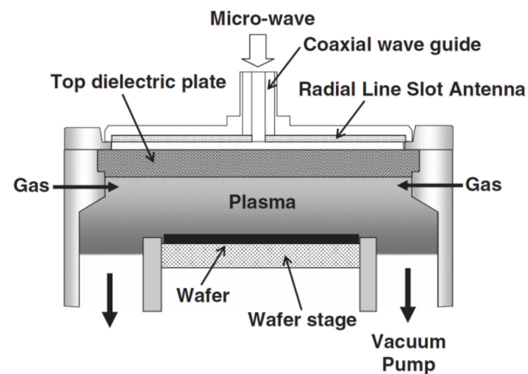

Figure 1: A cross-sectional view of RLSA™ PECVD reactor.

In dependence on governing mode, e.g. an interaction between electromagnetic (EM) wave and plasma, the SW plasma may exhibit some degree of spatial localization and allows separation of the location of plasma generation from the location of surface processing. Such behavior of SW plasma may have impact on the plasma chemistry either in the gas phase or on the surface. To explore and understand transient chemical vapor deposition (CVD) processes, such as atomic layer deposition (ALD), more knowledge is still required. Prediction of process results is not always straightforward, especially when new processes and films preparation involves much complex gas mixtures and specific process conditions.

Numerous studies were published on numerical modeling silane and hydrocarbons chemistry[2-21] in PECVD. Limited space of this paper does not allow list them all. Various dopant gas, hydrocarbons or other halocarbons

may be used as precursors to incorporate atoms into deposited film.

2. Model Description

In this paper, we present a two-dimensional axisymmetric model of microwave plasma produced by RLSA™ source and its numerical implementation under COMSOL Multiphysics. Plasma is sustained by 2.45 GHz EM wave distributed by antenna and propagating trough processing gas. The SW mode allows generation of uniform plasmas over several wavelengths of the EM wave (in vacuum $\lambda \sim 12.2$ cm). The EM waves cannot propagate in over-dense plasmas. The wave is reflected at the plasma surface due to the skin effect and becomes an evanescent wave. Its penetration depth into plasma corresponds to the skin depth. The non-vanishing penetration depth of an evanescent wave opens an alternative way of heating plasma. Instead of traversing the plasma (that is possible only below cutoff density ~ $7.5\text{x}10^{16}$ m^{-3}), the conductivity of the plasma enables the wave to propagate along the plasma surface. The wave energy is then transferred to the plasma by an evanescent wave which enters the plasma perpendicular to its surface and decays exponentially with the skin depth. Transfer mechanism allows generation of over-dense plasmas with electron densities beyond the critical density (above ~$3\text{x}10^{17}$ m^{-3}). Under certain conditions that are given by reactor size and geometry it can operate also in resonant mode or transitional mode. In the resonator mode, the plasma density does not exceed the critical density. A standing EM wave is confined by a reactor (resonator cavity) and penetrates the plasma which is sustained by wave in the regions of highest field intensity. The geometry of this region will determine the spatial distribution of the plasma.

SW-sustained discharges are structures which unify wave-fields and gas-discharge plasmas. The creation of these discharges is clear example of a self-consistent nonlinear problem: the wave produces the plasma and the plasma maintains the wave propagation. The discharge behavior is simultaneously governed by electrodynamics and gas discharge physics.[22] Solving large number of equations with complex chemistry and coupled wave-plasma physics at the scale of real reactor represents challenge.

2.1 Model geometry

The chamber geometry used for this model is shown in Fig. 2. We considered 2D model in axial symmetry. Plasma zone is represented by union of several domains with simple geometry and contains several probe domains to track plasma parameters. Typically, we were tracking local plasma density within probe domains and adjusted their position during solving different cases.

Diameter of modeled reactor is about 470 mm. The distance from window with RLSA antenna to wafer is approximately 130 mm. The RLSA™ source details on slot arrangements and their structure are not discussed in this work. We considered 2D interpretation of the antenna slot structure is good enough and adequate to approximate the azimuthal distribution of the microwave power into plasma.[23] In this paper we kept geometry fixed over the course of simulation work except minor refinements of specific geometrical features to sustain convergence of solution. Mostly, we have focused on plasma chemistry and its correlation to plasma parameters.

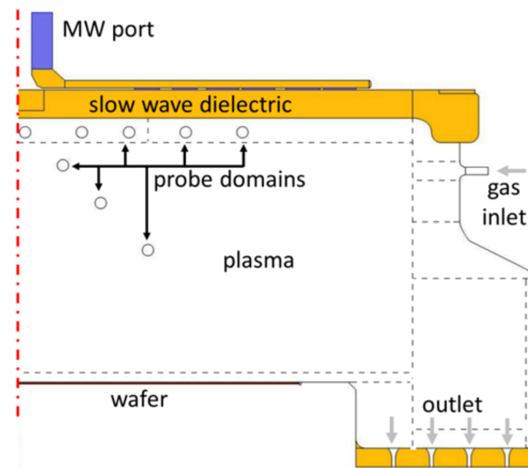

Figure 2: Domains in computational model (dashed lines represent interior boundaries in plasma).

2.2 Collisions and Volumetric Reactions

Gas mixture composition is important in film processing preparation. In such systems both primary (*i.e.*, electron-impact) and secondary (*i.e.*, homogeneous) reactions in the plasma play an important role. In particular, argon or hydro-

gen dilution of the source gas (typically, silane) influences the deposited film properties in significant way. Bombardment of the growing film by Ar ions and reactions of excited Ar with silane are responsible for the structural changes in film.[24] Precursors like SiH_2 or SiH_3 are directly or indirectly related to production and control film properties. Our motivation was to have insight and better understanding of the composition, spatial distributions and plasma parameters in presented reactor under various conditions and in variety of gas mixtures. Also complexity of chemical reactions at the surface is requiring further insight to understand mechanism.

Table 1: Collisions and reactions used in model: Argon.

Collision / Reaction Type	Formula		Refs.
Ionization (15.8 eV)	$e^- + Ar \rightarrow 2e^- + Ar^+$	R1-1	Ref.[28]
Elastic	$e^- + Ar \rightarrow e^- + Ar$	R1-2	
Excitation (11.5 eV, metastable substracted from total)	$e^- + Ar \rightarrow e^- + Ar^*$	R1-3	
Excitation metastable only (11.5 eV)	$e^- + Ar \rightarrow e^- + Ar^{*m}$	R1-4	
Quenching to resonant states rate constant ~2x10^{-7} cm^3s^{-1} for electron quenching to the "nearby" resonant states, average loss assumed ~ 3 eV	$e^- + Ar^{*m} \rightarrow e^- + Ar^*$	R1-5	Ref.[34]
Quenching to base state (-11.5 eV)	$e^- + Ar^{*m} \rightarrow e^- + Ar$	R1-6	Ref.[28]
Radiative recombination (10^{-11} cm^3s^{-1}, -4.3 eV)	$e^- + Ar^+ \rightarrow e^- + Ar^{*m} + h\nu$	R1-7	Ref.[35]
Penning ionization (3.734x10^8 $m^3s^{-1}mol^{-1}$)	$Ar^{*m} + Ar^{*m} \rightarrow e^- + Ar^* + Ar^+$	R1-8	
Metastable quenching (1807 $m^3s^{-1}mol^{-1}$)	$Ar^{*m} + Ar \rightarrow 2Ar$	R1-9	
Radiative decay (Estimate ~ 10^9 s^{-1})	$Ar^* \rightarrow Ar + h\nu$	R1-10	(a)
Stepwise ionization (E_{ion2}~4.427 eV)	$e^- + Ar^{*m} \rightarrow 2e^- + Ar^+$	R1-11	

NOTE: (a) estimate

Table 2: Collisions and reactions used in model: Hydrogen.

Collision / Reaction Type	Formula		Refs.
Elastic	$e^- + H_2 \rightarrow e^- + H_2$	R2-1	
Molecular ionization (Considered branching between H^+ and H_2^+ production)	$e^- + H_2 \rightarrow 2e^- + 0.07H +$ $+ 0.07H^+ + 0.93H_2^+$	R2-2	
Dissociative double ionization	$e^- + H_2 \rightarrow 3e^- + H_2^{2+} \rightarrow 3e^- + 2H^+$	R2-3	
Atomic ionization	$e^- + H \rightarrow 2e^- + H^+$	R2-4	
Molecular excitation	$e^- + H_2 \rightarrow e^- + H_2^{*(vib,el)}$	R2-5	Total
Dissociative excitation	$e^- + H_2 \rightarrow e^- + H_2^{*(vib,el)} \rightarrow e^- + 2H^*$	R2-6	
Dissociative ionization (rate constant ~2.1x10^{-9} cm^3s^{-1})	$H_2 + H_2^+ \rightarrow H + H_3^+$	R2-7	Ref.[39]

As for initial development the mixture of Ar, H_2, SiH_4, C_2H_6, and PH_3 dopant were selected. Other Si-based precursors might be under consideration, and in future work the Si-precursors with more complex structure will replace silane, e.g. either tetramethylsilane (TMS), e.g. $Si(CH_3)_4$, or trisilylamine (TSA) - $(SiH_3)_3N$. Reactions listed in Tables 1 to 5 represent baseline chemistry framework considered in model. They are sorted chronologically, in order as we build our model, overlooking for a moment an importance of individual reactions

and their role in process chemistry. We explore this approach as step towards testing capabilities of modeling approach by Comsol Multiphysics and extending our comprehension of chemical reactions in silane-containing systems.

In inert gas (argon) the formation of ions Ar^+ and excited atoms Ar^* due to collision with electrons depends upon applied microwave power density, and obviously, its spatial distribution is related to reactor size and geometry. Argon plasma was investigated in number of publications.[25-27] We used cross sections of electron-argon collisions (R1-1 to R1-11) that were obtained from MORGAN data at LXCat open-access database.[28] As we recognized later, more detailed Ar data set on excited argon is rather under HAYASHI[29] edition. Also we recommend recent publiccations[30-32] on proper interpretation and references to downloaded cross sections.

Values for many cross-sections are difficult to find. As an extension of model in this work, several reactions from metastable argon model[33] - electron quenching[34] to the "nearby" resonant states (R1-5) were considered. Rate constant for electron-ion radiative recombination (R1-7) was adopted from Ref.[35] Radiative decay of excited argon (R1-10) was estimated by rate 10^9 s^{-1}.

Table 3: Collisions and reactions used in model: Silane.

Collision / Reaction Type	Formula		Refs.
Attachment	$e^- + SiH_4 \rightarrow SiH_4^-$	R3-1	Ref.[29]
Elastic	$e^- + SiH_4 \rightarrow e^- + SiH_4$	R3-2	
Excitation E_{exc} ~ 0.115 eV, cross section E_{exc} ~ 0.27 eV, cross section E_{exc} ~ 8.01 eV, cross section E_{exc} ~ 8.92 eV, cross section	$e^- + SiH_4 \rightarrow e^- + SiH_4^*$	R3-3 R3-4 R3-5 R3-6	
Ionization E_{ion} ~ 12.9 eV, cross section	$e^- + SiH_4 \rightarrow 2e^- + SiH_4^+$	R3-7	
Dissociative ionization			Ref.[40] (a)
E_{ion} ~ 11.6 eV, k ~ 9.2x10^{-11} cm^{3}s^{-1}	$e^- + SiH_4 \rightarrow 2e^- + SiH_2^+ + H_2$	R3-8	
E_{ion} ~ 12.2 eV, k ~ 5.9x10^{-11} cm^{3}s^{-1}	$e^- + SiH_4 \rightarrow 2e^- + SiH_3^+ + H$	R3-9	
E_{ion} ~ 13.6 eV, k ~ 3.9x10^{-11} cm^{3}s^{-1}	$e^- + SiH_4 \rightarrow 2e^- + Si^+ + 2H_2$	R3-10	
E_{ion} ~ 15.1 eV, k ~ 3.4x10^{-12} cm^{3}s^{-1}	$e^- + SiH_4 \rightarrow 2e^- + SiH^+ + H_2 + H$	R3-11	
E_{ion} ~ 24.3 eV, k ~ 2.1x10^{-15} cm^{3}s^{-1}	$e^- + SiH_4 \rightarrow 2e^- + SiH_2 + H_2^+$	R3-12	
E_{ion} ~ 24 eV, k ~ 1.9x10^{-14} cm^{3}s^{-1}	$e^- + SiH_4 \rightarrow 2e^- + SiH_3 + H^+$	R3-13	
Dissociation, E_{diss}~4.0 eV, k ~ 1.59x10^{-10} cm^{3}s^{-1}	$e^- + SiH_4 \rightarrow e^- + SiH_3 + H$	R3-14	Ref.[41]
Dissociation, E_{diss}=2.2 eV, k ~ 1.87x10^{-11} cm^{3}s^{-1}	$e^- + SiH_4 \rightarrow SiH_2 + 2H + e^-$	R3-15	
Dissociation, E_{diss}=8.4 eV, k ~ 8.34x10^{-9} cm^{3}s^{-1}, (not included)	$e^- + SiH_4 \rightarrow SiH_4^* + e^-$	R3-16	
Dissociation, k ~ 1.4x10^{-10} cm^{3}s^{-1}	$Ar^{*m} + SiH_4 \rightarrow SiH_3 + H + Ar$	R3-17	
Dissociation, k~ 2.6x10^{-10} cm^{3}s^{-1}	$Ar^{*m} + SiH_4 \rightarrow SiH_2 + 2H + Ar$	R3-18	
E_a ~ 2.2 eV, k ~ 4x10^{-9} cm^{3}s^{-1}	$e^- + SiH_4 \rightarrow e^- + SiH_2 + H_2$	R3-19	Refs.[42,43,44] (b)
E_a ~ 4.0 eV, k ~ 1.5x10^{-9} cm^{3}s^{-1} (not included)	$e^- + SiH_4 \rightarrow e^- + SiH_3 + H$	R3-20	
E_a ~ 4.2 eV, k ~ 6.6x10^{-11} cm^{3}s^{-1}	$e^- + SiH_4 \rightarrow e^- + Si + 2H_2$	R3-21	
E_a ~ 5.7 eV, k ~ 4.3x10^{-11} cm^{3}s^{-1}	$e^- + SiH_4 \rightarrow e^- + SiH + H_2 + H$	R3-22	
E_a ~ 9.5 eV, k ~ 7.1x10^{-12} cm^{3}s^{-1}	$e^- + SiH_4 \rightarrow e^- + Si^* + 2H_2$	R3-24	
E_a ~ 8.9 eV, k ~ 1.0x10^{-11} cm^{3}s^{-1}	$e^- + SiH_4 \rightarrow e^- + SiH^* + H_2 + H$	R3-25	

NOTE: (a) measured in Ar at room T,1 Pa 500 sccm, 300 W; (b) Dissociation (room temperature, T_e~1.8 eV)

Table 4: Collisions and reactions used in model: Ethane.

Collision / Reaction Type	Formula		Comment
Elastic	$e^- + C_2H_6 \rightarrow e^- + C_2H_6$	R4-1	0.03065 kg/mol; 1.823x10^{-5}; Kihara[51] potential characteristic length 3.1A; potential energy minimum $\varepsilon/k_B \sim 420$ K
Excitation	$e^- + C_2H_6 \rightarrow e^- + C_2H_6$	R4-2 R4-3 R4-4 R4-5	$E_{exc\ (vib\ 24)} \sim 0.16$ eV $E_{exc\ (vib\ 13)} \sim 0.371$ eV $E_{exc} \sim 7.53$ eV $E_{exc} \sim 10.12$ eV
Ionization	$e^- + C_2H_6 \rightarrow 2e^- + C_2H_6^+$	R4-6	12.7 eV
Attachment	$e^- + C_2H_6 \rightarrow C_2H_6^-$	R4-7	Ref. [29]

Table 5: Collisions and reactions used in model: Phosphine.

Collision / reaction type	Formula		Comment
Elastic	$e^- + PH_3 \rightarrow e^- + PH_3$	R5-1	[(a)]
Ionization	$e^- + PH_3 \rightarrow 2e^- + PH_3^+$	R5-2	
Excitation	$e^- + PH_3 \rightarrow e^- + PH_3^*$	R5-3	
dissociation	$e^- + PH_3 \rightarrow e^- + PH_2 + H$	R5-4	
attachment	$e^- + PH_3 \rightarrow +PH_3^-$	R5-5	

[(a)]NOTE: 0.03399758 kg/mol; Dipole moment 0.58 D

Adding hydrogen generates a number of molecules in various excitation states. We implemented complete reaction set for electron-neutrals collisions from IST-LISBON database on the LXCat open-access website.[36] Measurements of very-high-frequency hydrogen plasmas[37] determined that ion species are dominated by H_2^+ at low pressure (<20 mTorr), whereas at high pressure by H_3^+ due to reaction (R2-7). Rest of homogeneous reactions were taken from model[38] reported earlier. In attempt to reduce stiffness of numerical system and still account correctly for electron energy balance, we consider multiple reactions producing excited atoms or molecules in various stage, however, assigned them formally to singular "effective" atom or molecule, e.g. H^{exc} or H_2^{exc} within a model.

In plasma, excited molecules SiH_4^* (R3-3 to R3-6), positive SiH_4^+ (R3-7) and negative SiH_4^- (R3-1) ions are produced by primary collisions of electrons with silane molecules. We used cross sections for collisions of electron with silane from LXCat open-access database[29], reactions (R3-1 to R3-16). Electron-impact dissociation rates at room temperature were taken from Refs.[41,45] Principle reactions related to forming radicals from silane[41] are due to electron collisions as well (R3-14 to R3-16). Radical SiH* is mainly due to dissociative de-excitation (R3-29 and R3-31). However, in mixture with argon, the loss mechanism of Ar* is representing an opportunity for production of radicals (at high dilution by argon) from silane by reactions (R3-17) or (R3-18). Within a scope of this paper we focused only on implementation of reactions in a numerical model, without judgment on their proper use. In this manner we included relevant homogeneous gas-phase reactions from Table 2. in Ref.[45] (values at room temperature), in this paper labeled as Table. 3. In further work rate constants were implemented in terms of Refs.[15,46]

The electron-neutral cross sections for next component in the mixture – ethane (C_2H_6) - were gained from HAYASHI[29] on-line edition at LXCat, these are listed briefly above in Table 4. Gas phase reactions were taken from Refs.[47-49] phosphine (PH_3) related reactions[50] are listed in Table 5.

In present model only several surface reactions were considered to explore model into prediction of deposited film composition. Initially, a sticking coefficient was considered it has value 1. Demand for computational resources increased tremendously with increase of number of

species in model. Number of reactions had less significant impact. That was one of the reason that we decided not to increase complexity further with surface species until routine convergence of current reaction scheme will be achieved in reasonable range of the process conditions. Most of simulation was done in simple chemistry ($Ar + H_2$) and more complex chemistry is ongoing.

3 Use of COMSOL Multiphysics

In this work we explored capabilities and easy to use GUI of Plasma Module in COMSOL Multiphysics suite ver.4.3.b. The numerical modeling of reactive CVD process commonly involves the solution of multiple convection-diffusion reaction equations for a large number of reactants and intermediate species. These equations are firmly coupled through the reaction terms with tens of finite rate elementary reaction steps and largely varying rate constants. The solution of such rigid sets of equations is difficult, especially when time-accurate transient solutions are required. Moreover, the plasma is created by the EM wave but it also reflects and guides this same wave. Therefore, a truly self-consistent description is necessary and numerical modeling is quite involved in design. Since electron energy distribution function (EEDF) has impact on plasma chemistry by using easy formulation in COMSOL Multiphysics we did attempt to look briefly into difference in results when replacing Maxwell-Boltzman (MB) by Druyvesteyn distributions. This assumption might cause disagreement between model and experiment. Inherently, the RF and AC/DC modules are included into numerical formulation of plasma. Further, compressible flow ($M<3$) module was coupled with plasma module and solved in self-consistent manner. We considered reactor at constant temperature, e.g. the rate constants in presented model are not function of temperature. Thermal module will be coupled to system of convection-diffusion reaction equations at later phase.

4. Results and Discussion

In this section we are presenting initial results computed by model. Dell Precision WorkStation T7500 (64bit Windows 7 Enterprise OS, two processors X5690 – 24 cores, RAM 96 GB) was used for computation. Demand for RAM when computing individual cases was in range from 10 to 50 GB, computational time from 4 hours to over 100 hours per case, in dependence on conditions for plasma in model and components in gas mixture. Individual cases converged typically very well at times in range from 1 to 10 ms. Computation of some cases did not progress well around interval between 1-5 µs and transient solution was computed very slowly (>100 hours) with time steps $\Delta t \sim 10^{-19} – 10^{-15}$ s. We did not investigate reason why, though we believe, this might be related to ion transport. We were not always successful with mesh refinement or smoothing geometry to gain on convergence. Initial conditions were the most sensitive factor that have impact on convergence of stiff equation system and achieve solution, especially in cases with more than two-component mixtures. Initial cases contained argon collisions only. Adding hydrogen increased substantially number of reactions.

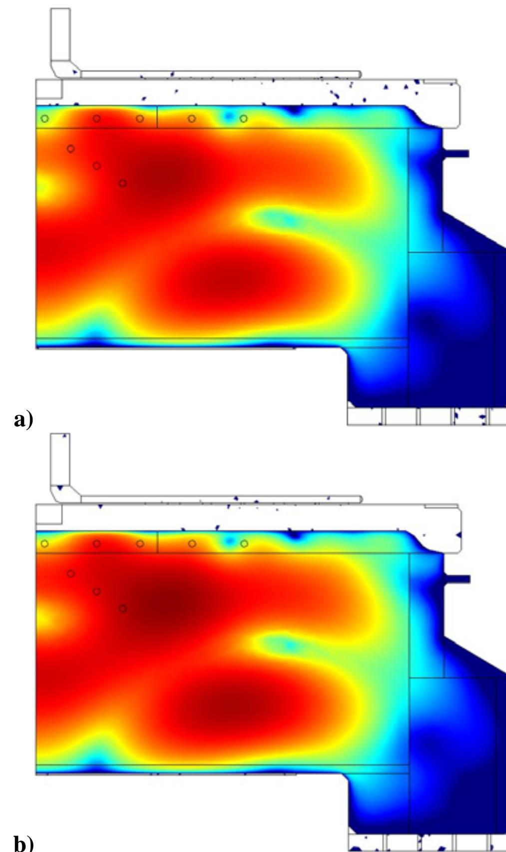

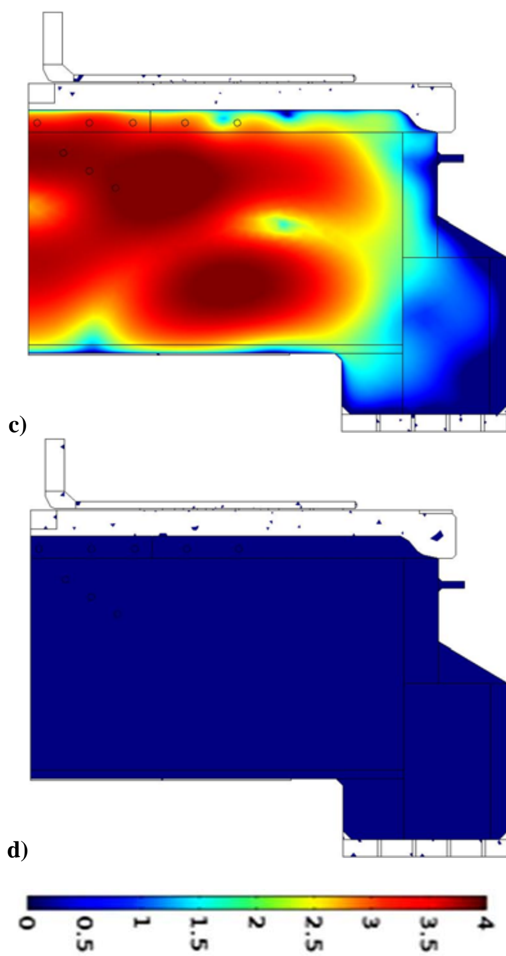

Figure 3: Surface plots of log values for resistive loss in plasma in Wm^{-3}: (a) 100 % Ar; (b) 5 % H_2 in Ar; (c) 20 % H_2 in Ar and (d) above 40 % H_2 in Ar. Color scale is same for all plots in range from 0 to 4 Wm^{-3}. Unit of resistive loss (Q_{rh}) is Wm^{-3}: Individual cases converged typically in range 1 - 10 ms.

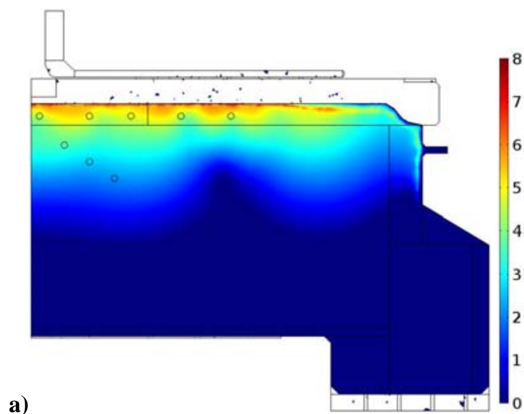

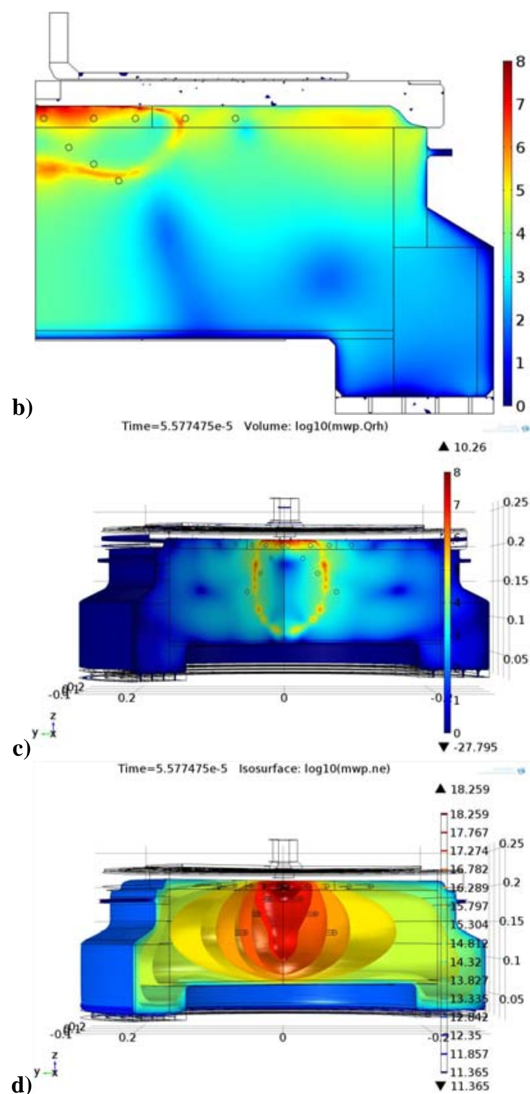

Figure 4: Surface plots of log values for resistive loss in 5 % H_2 in Ar plasma: (a) 500 mTorr; (b) 200 mTorr; and (c) 100 mTorr Color scale is same for all plots in range from 0 to 4 Wm^{-3}. Unit of resistive loss (Q_{rh}) is Wm^{-3}. (d) Iso-surface plots of electron density (n_e, m^{-3}) in $Ar+H_2+SiH_4$ plasma at 100 mTorr. Hydrogen and silane flows were sustained at low level to enable convergence. NOTE: Case was interrupted due to computation time over 100 hours.

To investigate an impact of $Ar + H_2$ mixture composition on resistive heating we computed various ratio of $Ar+H_2$ plasma at 50 mTorr. Microwave power was 3500 W and total flow 400 sccm. Surface plots in Fig. 3 illustrate resistive heating on $\log_{10}(Q_{rh})$ scale, where Q_{rh} is in Wm^{-3}. At initial low ratios of hydrogen in

argon, the resistive losses were increasing with H_2 flow, however at 40 % H_2 in Ar and above the Q_{rh} dropped to very low values ~10^{-3} Wm^{-3} and in fact plasma was diminished according model. At value 60 % reached a minimum value in this sequence Q_{rh} ~10^{-7} Wm^{-3}, and at 80 % H_2 again Q_{rh} ~ 10^{-3} Wm^{-3}.

There was an assumption that plasma will reignite in pure H_2. We did complete this series with pure H_2 only case, however, our assumption was not confirmed. Either increase in microwave power to 7 kW or setting sticking coefficients for recombination of excited and ionized hydrogen on reactor surface did not have an impact, and resistive losses remained low at ~ 10^{-3} Wm^{-3}. Reduction of flow rate to 1sccm did not have impact as well on Q_{rh}. From model it follows that at these conditions wave propagates through plasma in transitional regime. The wave structure in reactor was almost stable, and only weakly coupled to plasma.

Investigating plasma profile *vs.* pressure is illustrated in Fig. 4. Again, we assumed 5 % H_2 in Ar mixture. At high pressure, 500 mTorr, resistive losses occur closely to dielectric window, peaking up to 8.9 Wm^{-3}. Electron density and temperature under these conditions are presented Fig. 5-a, where T_e at window location is about 5-times higher than T_e at the wafer. Due to this over-dense plasma is produced reaching up to $6x10^{13}$ cm^{-3}.

In Fig. 4-b, the resistive losses at 200 mTorr do not occur on whole window, rather, they are closing boundary around over-dense plasma (Fig. 5-b). This effect is well demonstrated 100 mTorr (Fig. 4-c). The 50 mTorr case we presented in Fig. 3-b, and plasma at 20 mTorr case was coupled very weakly to wave.

Described model is not completed in sense of detailed surface chemistry and anticipated full chemistry scale. This is currently undergoing work. Also certain assumptions were made to overcome the absence of rate constants or cross sections data. Mixed data sets were used and do not include dependence on temperature. Below are more critical limitations or assumptions made in described model:

a) Fast atoms produced in charge exchange collisions present in plasma were not considered (for instance, fast hydrogen atoms or molecules)

b) The importance[45] of fast electron tail in EEDF (20 – 40 eV) – a result of production of fast electrons in collision with heavy species is responsible for recovering part of electron energy.

c) Below 10 mTorr pressure – a gas flow is in viscous-molecular regime.

d) High pressures reactions are neglected, they cause formation of polysilanes and are usually not suitable for high-quality films, though they have presence in processing zone.

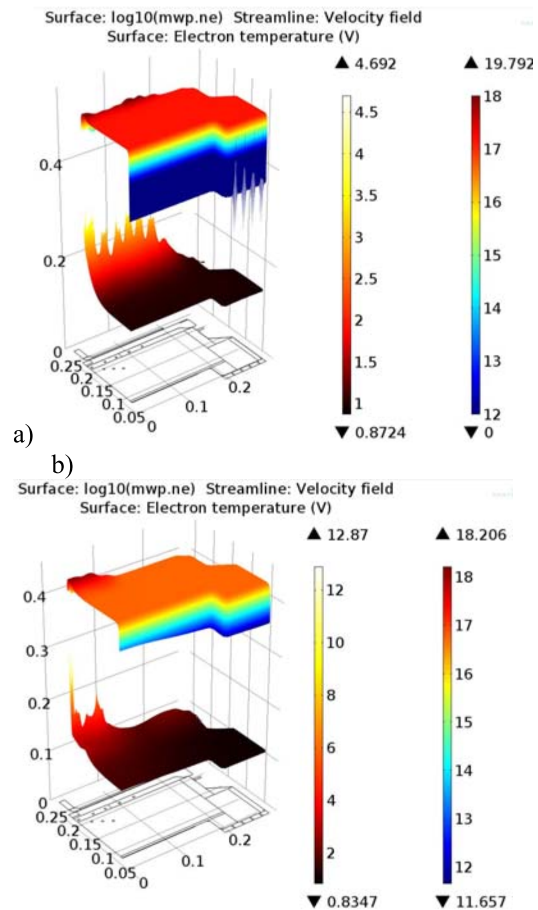

Figure 5: Surface plots of electron density, n_e, and electron temperature, T_e, in 5 % H_2 +Ar mixture (total flow was 400 sccm, microwave power 3500 W): (a) 500 mTorr converged case; (b) 200 mTorr (not fully converged, interrupted at 1.9 µs).

Computed results might underestimate the real plasma properties due to absence of fast species, energy transfer back to electrons in collisions with atoms, transport behavior of fast species. On another side model is very useful in enabling better understanding of chemistry. For instance, in Fig. 6, several parameters in plasma

at low pressure (<50 mTorr) operation in Ar $+H_2$ mixture are illustrated. Microwave power is propagating from coaxial inlet into "slow wave structure" above the actual plasma inside reactor. It cannot propagate deeper into dense plasma and actually travels as surface wave around plasma core defined by critical plasma density. Surface plot inside reactor illustrate resistive heating in plasma. Streamlines show flux of charged particles out of the plasma towards the surrounding walls.

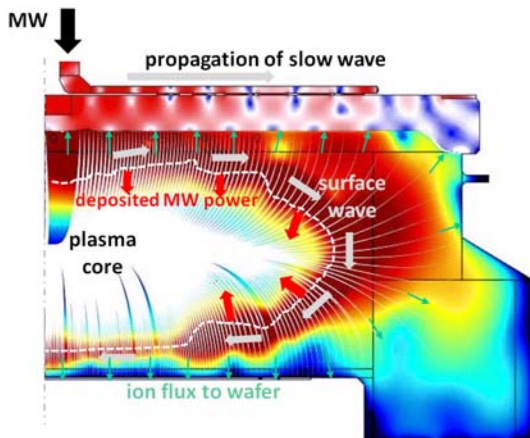

Figure 6: Principal domains assumed in film stack model.

5. Conclusions

In summary, the comprehensive assessment of particular cases with an immediate access to detailed information are attractive to research and engineering environment. In the course of simulation we were evaluating computational resources and capabilities of such approach within industrial environment. Computational times are sensitive to process conditions, providing fast turnover at reduced pressures and reasonable reaction sets. More robust reaction schemes and pressures above 100 mTorr are demanding much larger computing resources. On process side this model successfully predicts the spatial distributions of multiple components in complex molecular plasma. On hardware side (semiconductor tool configuration) it gives substantial flexibility to additional modifications of reactor configuration without time-consuming reworks.

8. References

1. H. Ueda, Y. Ohsawa, Y. Tanaka, and T. Nozawa, High-quality SiO_2 film formation below 400 °C by PECVD using tetraethoxysilane source gas, *Jap. Jour. Applied Physics* **48**, 126001 (2009).
2. A. Salabas, G. Gousset, L. L. Alves, *Plasma Sources Sci. Technol*. **11**, 448 (2002).
3. G. J. Nienhuis, W. Goedheer, *Plasma Sources Sci. Technol.* **8**, 295 (1999).
4. M. J. Kushner, J. Appl. Phys. **71**, 4173 (1992).
5. K. De Bleecker, D. Herrebout, A. Bogaerts, R. Gijbels, P. Descamps, *J. Appl. Phys.* **36**, 1826 (2003).
6. J. Perrin et al., *J. Vac. Sci. Technol.* **A16**(1), 278 (1998).
7. O. Leroy, G. Gousset, L. L. Alves, J. Perrin, J. Jolly, *Plas. Sour. Sci. Technol.* **7**, 348 (1998).
8. Y. Yasaka, A. Fukuyama, A. Hatta, R. Itatani, *J. Appl. Phys.* **72**, 2652 (1992).
9. T. Morimoto, Y. Yasaka, M. Tozawa, T. Akahori, H. Amano, N. Ishii, *Jpn. J. Appl. Phys.* **36**, 4769 (1997).
10. Y. Yasaka, N. Uda, *J. Appl. Phys.* **89**, 3594 (2001).
11. Y. Miyamoto, Y. Tamai, K. Daimon, M. Esaki, H. Takeno, Y. Yasaka, *Thin Solid Films* **506-507**, 622 (2006).
12. K. Tao, D. Mao, J. Hopwood, *J. Appl. Phys.* **91**, 834 (2002).
13. A. V. Vasenkov, M. J. Kushner, *J. Appl. Phys.* **95**, 4040 (2004).
14. H. Yamada, A. Chayahara, Y. Mokuno, Y. Soda, Y. Horino, N. Fujimori, *Diam. Relat. Mater.* **14**, 1776 (2005).
15. Amatnatides, Stamou and Mataras, *J. Appl. Phys.* **90** 5789 (2001).
16. S. Nakamura et al., *Journal of Non-Crystalline Solids* **352** 919-924 (2006).
17. G.M. Petrov and J.L. Giuliani, Model of two stage rf plasma reactor for SiC deposition, *Journal of Applied Physics* **90** 619-636 (2001).
18. T. Shirafuji, k. Tachibana and Y. Matsui, Measurement and calculation of SiH_2 radical density in SiH_4 and $Si2H_6$ plasma for the deposition of hydrogenated amorphous silicon thin films, *Jpn. J. Appl. Phys*. **34** 4239-4246 (1995).
19. T. Takahashi et al., The effect of gas-phase additives C_2H_4, C_2H_6 and C_2H_2on SiH_4/O_2 CVD, *J. Electrochem. Soc.* 1**43** 1354-1361 (1996).

20. M.D. Allendorf and R. J. Knee, A model of SiC CVD, *J. Electrochem. Soc.* **138** 841-852 (1991).
21. P.M. Lofgren, W. Ji, C. Hallin and C.-Y. Gu, Modeling of SiC epitaxial growth in hot-wall CVD processes, *J. Electrochem. Soc.* **147** 164-175 (2000).
22. Yu.M. Alievev, H. Schlüter and A. Shivarova, Guided-wave-produced plasmas, *Springer-Verlag Berlin Heidelberg* (2000).
23. J. Brcka and S.Y. Kang, Multiphysics coupling simulation of silicon nitride CVD using an RLSA source, *Plasma Process. Polym.* **6**, S776-S783 (2009).
24. P.P. Ray and P. Chaudhuri, Study of RF plasma of silane – argon mixture by OES, *Czechoslovak Jour. of Physics* **50** Suppl. S3 (2000).
25. MORGAN database, www.lxcat.laplace.univ-tlse.fr
26. A. Bogaerts and R. Gijbels, Description of the argon-excited levels in a radio-frequency and direct current glow discharge, *Spectrochimica Acta* Part **B55** 263-278 (2000).
27. A.I. Strinic, G.N. Malovic, Z.Lj. Petrovic, and N. Sadeghi, Electron excitation coefficients and cross sections for excited levels of argon and xenon ions, *Plasma Sources Sci. Technol.* **13** 333-342 (2004).
28. MORGAN database, www.lxcat.laplace.univ-tlse.fr
29. HAYASHI database, www.lxcat.laplace.univ-tlse.fr ; Hayashi (2003), table 2.
30. L.C. Pitchford, L.L. Alves, K. Bartschat, S.F. Biagi, M.C. Bordage, A.V. Phelps, C.M. Ferreira, G.J.M. Hagelaar, W.L. Morgan, S. Pancheshnyi, V. Puech, A. Stauffer and O. Zatsarinny, Comparisons of sets of electron-neutral scattering cross sections and swarm parameters in noble gases: I. Argon, *J. Phys. D: Appl. Phys.* **46** 334001 (2013).
31. L.L. Alves, K. Bartschat, S.F. Biagi, M.C. Bordage, L.C. Pitchford, C.M. Ferreira, G.J.M. Hagelaar, W.L. Morgan, S. Pancheshnyi, A.V. Phelps, V. Puech and O. Zatsarinny, Comparisons of sets of electron-neutral scattering cross sections and swarm parameters in noble gases: II. Helium and neon, *J. Phys. D: Appl. Phys.* **46** 334002 (2013).
32. M.C. Bordage, S.F. Biagi, L.L. Alves, K. Bartschat, S. Chowdhury, L.C. Pitchford, G.J.M. Hagelaar, W.L. Morgan, V. Puech and O. Zatsarinny, Comparisons of sets of electron-neutral scattering cross sections and swarm parameters in noble gases: III. Krypton and xenon, *J. Phys. D: Appl. Phys.* **46** 334003 (2013).
33. A. Bogaerts and R. Gijbels, Modeling of metastable argon atoms in a direct current glow discharge, *Physical Review* **A 52**, 3744 (1995)
34. D.P. Lymberopoulos and D.J. Economou, J. Appl. Phys. **73**, 3668 (1993).
35. M.A Biondi, *Physical Review* **129**, 1181 (1963).
36. IST-LISBON database, www.lxcat.laplace.univ-tlse.fr; Yanguas-Gil et al. (2005).
37. S. Nunomura and M. Kondo, Characterization of high-pressure capacitively coupled hydrogen plasmas. *Journal of Applied Physics* **102**, 93306 (2007).
38. Brcka J., Modeling remote H_2 plasma in semiconductor processing tool. Proc. of the COMSOL Users Conference, pp. 431-436, Boston, USA, (Oct 2006).
39. H. Tawara et al., Cross sections and related data for electron collisions w hydrogen molecules and molecular ions. *J. Phys. Chem. Data* **19** (1990).
40. R. Basner et al., *Int. J. Mass Spectrom. Ion Process* **171** 83 (1997).
41. M.J. Kushner, J. Appl. Phys. **63** (1988) 2532.
42. F.J. Kampas, *Semicond. Semimet.* 21A 153 (1984).
43. M. Hirose, *Semicond. Semimet.* **21A** 9 (1984).
44. Perrin, J.P.M. Schmitt, *Chem. Phys.* **67** 167 (1982).
45. A.Y. Kovalgin et al., Chemical modeling of a high-density ICP plasma reactor containing silane, *Surface & Coating Technology* **201**, 8849-8853 (2007).
46. S. Nakamura, K. Matsumoto, A. Susa and M. Koshi, Reaction mechanism of silicon Cat-CVD, *Journal of Non-Crystalline Solids* **352** 919-924 (2006).
47. A. Dollet et al., Simulation of SiC deposition from $SiH_4/C_3H_8/Ar/H_2$ mixtures in a cold–wall CVD reactor, *Surface and Coating Technology* **177-178** 382-388 (2004).
48. A. Veneroni, F. et al., Epitaxial deposition of SiC films in a horizontal hot-wall CVD reactor, *Materials Science Forum* **483-485** 57-60 (2005).
49. A. Fiorucci, D.Moscatelli, M. Masi, Homoepitaxial silicon carbide deposition processes via chlorine routes, *Surface Coating and Technology* **201** 8825-8829 (2007).
50. T. Kihara, *Adv. Chem. Phys.* 5, 147 (1964).